THE JOURNAL OF BIOLOGICAL CHEMISTRY VOL. 287, NO. 44, pp. 37233–37244, October 26, 2012

Bidirectional Coupling between Ryanodine Receptors and Ca^{2+} Release-activated Ca^{2+} (CRAC) Channel Machinery Sustains Store-operated Ca^{2+} Entry in Human T Lymphocytes[S]

Received for publication, July 6, 2012, and in revised form, August 29, 2012 Published, JBC Papers in Press, September 4, 2012, DOI 10.1074/jbc.M112.398974

Pratima Thakur, Sepehr Dadsetan, and Alla F. Fomina[1]

From the Department of Physiology and Membrane Biology, University of California, Davis, California 95616

Background: Ryanodine receptors (RyR) are intracellular Ca^{2+} release channels.
Results: RyR are expressed in human T cells. Modulating the RyR activity in human T cells affects Ca^{2+} leakage from the store and store-operated Ca^{2+} entry.
Conclusion: RyR strongly regulate Ca^{2+} influx in human T cells.
Significance: RyR can be used as a target for manipulating immune responses in humans.

The expression and functional significance of ryanodine receptors (RyR) were investigated in resting and activated primary human T cells. *RyR1*, *RyR2*, and *RyR3* transcripts were detected in human T cells. *RyR1/2* transcript levels increased, whereas those of *RyR3* decreased after T cell activation. RyR1/2 protein immunoreactivity was detected in activated but not in resting T cells. The RyR agonist caffeine evoked Ca^{2+} release from the intracellular store in activated T cells but not in resting T cells, indicating that RyR are functionally up-regulated in activated T cells compared with resting T cells. In the presence of store-operated Ca^{2+} entry (SOCE) via plasmalemmal Ca^{2+} release-activated Ca^{2+} (CRAC) channels, RyR blockers reduced the Ca^{2+} leak from the endoplasmic reticulum (ER) and the magnitude of SOCE, suggesting that a positive feedback relationship exists between RyR and CRAC channels. Overexpression of fluorescently tagged RyR2 and stromal interaction molecule 1 (STIM1), an ER Ca^{2+} sensor gating CRAC channels, in HEK293 cells revealed that RyR are co-localized with STIM1 in the puncta formed after store depletion. These data indicate that in primary human T cells, the RyR are coupled to CRAC channel machinery such that SOCE activates RyR via a Ca^{2+}-induced Ca^{2+} release mechanism, which in turn reduces the Ca^{2+} concentration within the ER lumen in the vicinity of STIM1, thus facilitating SOCE by reducing store-dependent CRAC channel inactivation. Treatment with RyR blockers suppressed activated T cell expansion, demonstrating the functional importance of RyR in T cells.

T lymphocytes play a central role in cell-mediated immunity. T cells express T cell receptors that bind antigens displayed on the surface of antigen-presenting cells (APC)[2] (1, 2). Stimulation of naive or memory resting T cells with a specific antigen or a nonspecific mitogen alters the expression of different genes, a process known as activation (3–9).

Activated T cells follow very typical response patterns (2). An initial phase consists of massive expansion of an antigen-specific T cell population. The expansion phase is followed by activated T cell differentiation into effector T cell subsets committed to secrete a variety of cytokines, which modulate the functions of other cells of the immune system. Although expansion of T cells specific for the target pathogen is crucial for mounting an effective immune response to active infection, the expansion of T cells specific to a self-antigen or environmental allergen may cause immuno-mediated diseases (10, 11). Gaining insight into the mechanisms governing T cell activation is thus critical to the development of specific therapeutic strategies to control T cell-mediated immune responses.

Elevation in cytosolic Ca^{2+} concentration ($[Ca^{2+}]_i$) is crucial for T cell activation (3). Store-operated Ca^{2+} entry (SOCE) via plasmalemmal Ca^{2+} release-activated Ca^{2+} (CRAC) channels activated in response to depletion of the intracellular Ca^{2+} store (mostly endoplasmic reticulum (ER)) is a major source for $[Ca^{2+}]_i$ elevation in T cells. T cells with impaired SOCE fail to expand and secrete cytokines upon activation, leading to immunodeficiency and autoimmune disorders in humans and mice (12, 13). Having the tools for pharmacological manipulation of T cell SOCE would be beneficial for modifying immune responses in humans. However, identifying compounds that directly or indirectly selectively modulate T cell CRAC channel activity and are suitable for application in humans has been elusive (14–17). Here, we explored the dependence of T cell SOCE on ryanodine-sensitive Ca^{2+} release channels, also known as ryanodine receptors (RyR), whose activity can be altered in a predictable manner by clinically relevant drugs, such as caffeine and dantrolene.

[S] This article contains supplemental Fig. 1.

[1] To whom correspondence should be addressed: Dept. of Physiology and Membrane Biology, University of California, One Shields Ave., Davis, CA 95616-8644. Fax: 530-752-5423; E-mail: affomina@ucdavis.edu.

[2] The abbreviations used are: APC, antigen-presenting cell(s); RyR, ryanodine receptor(s); SOCE, store-operated Ca^{2+} entry; CRAC, Ca^{2+} release-activated Ca^{2+}; ER, endoplasmic reticulum; CICR, Ca^{2+}-induced Ca^{2+} release; C_q, quantification cycle; Ry, ryanodine; DS, dantrolene sodium; SERCA, sarco/endoplasmic reticulum Ca^{2+} ATPase; CPA, cyclopiazonic acid; $[Ca^{2+}]_{ER}$, Ca^{2+} concentration within the endoplasmic reticulum lumen; CFSE, carboxyfluorescein diacetate succinimidyl ester; IP3R, inositol 1,4,5-trisphosphate receptor.

Previous studies performed on Jurkat T cells, a human lymphoblastic leukemia T cell line, suggested that RyR may be involved in regulating Ca^{2+} signaling in T cells (18–24). We have previously shown that in Jurkat T cells, the RyR regulate SOCE by controlling Ca^{2+} store refilling (19). However, the conclusions drawn from studies on Jurkat T cells cannot be extended to primary human T cells because the latter express type 1 RyR (RyR1) and type 2 RyR (RyR2), whereas Jurkat T cells express type 3 RyR (RyR3) (25). Furthermore, T cell lines are not representative of any functional state typical of primary T cells and do not respond to stimulation in the same manner as primary T cells. Thus, the functional significance of RyR in primary human T cells has not been elucidated.

Accordingly, we designed this study to understand the mechanism of action and functional significance of RyR in primary human T cells. We found that RyR strongly regulate SOCE in activated but not resting T cells. Furthermore, inhibiting RyR activity reduces activated T cell expansion *in vitro*. Our study provides evidence that RyR are bidirectionally coupled to CRAC channel machinery such that SOCE mediated via CRAC channels activates RyR by a Ca^{2+}-induced Ca^{2+} release (CICR) mechanism, which in turn reduces the Ca^{2+} concentration in the vicinity of the CRAC channel ER Ca^{2+} sensor stromal interaction molecule 1 (STIM1) to limit store-dependent CRAC channel inactivation and sustain SOCE.

EXPERIMENTAL PROCEDURES

Human T Cell Culture and Chemicals—Peripheral blood samples were collected from healthy subjects of both sexes and different ethnic backgrounds. All procedures involving human subjects were approved by the University of California Davis Internal Review Board. Blood was collected into sodium heparin-containing collection tubes (BD Biosciences), and then resting T cells were purified from whole blood by the negative selection method using RosetteSep® human T cell enrichment mixture (StemCell Technologies, Vancouver, Canada) and RosetteSep® density medium (StemCell Technologies) according to the manufacturer's instructions. After isolation, resting T cells were kept at a density of 0.5×10^6 cells/ml in cell culture medium containing RPMI 1640 medium with glutamine and HEPES (Lonza/BioWhittaker, Basel, Switzerland), supplemented with 10% FBS (Omega Scientific, Tarzana, CA), 2% GlutaMAX (Invitrogen), 1% RPMI 1640 vitamin solution, 1% RPMI 1640 amino acid solution, 1% sodium pyruvate, 0.03% β-mercaptoethanol. A portion of the resting T cells was used for experiments within 48 h after isolation. Another portion of the resting T cells was activated by anti-CD3 mAbs (Miltenyi Biotech, Auburn, CA) coated on cell culture dishes and by soluble anti-CD28 mAb (1–5 μg/ml; Miltenyi Biotech). The activated T cells were collected for experiments 4–5 days after activation when they were in the logarithmic phase of growth. Both resting and activated T cells were kept in 5% CO_2 at 37 °C; activated T cells were split every 2 days.

Unless otherwise indicated, all chemicals were from Sigma-Aldrich; dantrolene sodium (DS) and ionomycin were from Calbiochem; ryanodine (Ry) was from Calbiochem or Alamone (Jerusalem, Israel); Fura-2/AM and pluronic F-127 were from Molecular Probes, Inc. (Eugene, OR). Stock solutions of Ry (10 mM) and DS (10 mM) were prepared in methanol and DMSO, respectively.

RT-PCR Analyses—Assays were performed as described previously (26). Briefly, total RNA was extracted from cell lysates using a 6100 Nucleic Acid PrepStation (Applied Biosystems, Foster City, CA) according to the manufacturer's instructions. First-strand cDNA was generated using the QuantiTect Reverse transcription kit (Qiagen, Valencia, CA) according to the manufacturer's instructions. All samples were preamplified using the Advantage 2 PCR enzyme system (Clontech, Mountain View, CA) and the conditions described by Dolganov *et al.* (27). Dilutions of 1:100 of the preamplified material were used for the RT-PCR analyses. Human RT-PCR gene expression assays used for *RyR1* (Hs00166991_m1), *RyR2* (Hs00892902_m1), *RyR3* (Hs01050911_m1), β_2-microglobulin (*B2M*; Hs99999907_m1), and ribosomal protein L13a (*RPL13a*; Hs01926559_g1) were obtained from Applied Biosystems.

For quantitative RT-PCR, 5 μl of the diluted cDNA sample was added to a TaqMan Fast Universal PCR Master Mix (Applied Biosystems) and TaqMan Gene Expression Assay primer/probe mixes to achieve a final reaction volume of 12 μl. Negative controls were performed using sterile water instead of cDNA templates. The samples were placed in wells of a 384-well plate and amplified in an automated fluorometer ABI PRISM 7900 HTA FAST real-time PCR system (Applied Biosystems). Amplification conditions were as follows: 2 min at 50 °C, 10 min at 95 °C, 40 cycles of 15 s at 95 °C and 60 s at 60 °C. Fluorescence signals were collected during the annealing temperature, and raw quantification cycle (C_q) values were exported with a threshold of 0.1 and a base line of 3–10 for the genes of interest (GOI) and a range of 1–4 for the housekeeping genes. All analyses were performed in duplicate.

The comparative C_q method (28) was used to calculate linearized levels of each gene of interest relative to the geometric average of two stably expressed housekeeping genes *B2M* and *RPL13a* (26) using the formula, linearized levels of GOI relative to housekeeping genes $= 2^{-\Delta C_q}$, where ΔC_q is as follows.

$$\Delta C_q = C_{q\mathrm{GOI}} - \sqrt{C_{qB2M} \times C_{qRPL13a}} \qquad \text{(Eq. 1)}$$

The S.D. values of the raw C_q values of *B2M* and *RPL13a* in all samples used in this study were 0.63 and 0.78 ($n = 16$), respectively, whereas the Pearson correlation coefficient was 0.77.

Immunostaining—Resting or activated T cells were plated on poly-L-lysine-coated coverslips and fixed with 4% paraformaldehyde in PBS for 30 min, washed three times with 2× PBS, and permeabilized for 1 h in 0.075 (% w/v) saponin solution in 2× PBS. Cells were blocked in 5% (v/v) goat serum and 5% (w/v) bovine serum albumin in 2× PBS for 1 h at 21 °C. Coverslips were incubated overnight at +4 °C with primary mouse mAb 34C (1:10 concentrate dilution; Developmental Studies Hybridoma Bank, University of Iowa, Iowa City, IA), which recognizes RyR1 and RyR2 isoforms in a variety of species (29–32). Mouse IgG1 mAb (Invitrogen) was used as a negative control to assess the level of nonspecific binding of 34C mAb to human T cells. Coverslips were washed three times with 2× PBS and goat anti-mouse Alexa Fluor 488-conjugated secondary Ab (1:1000 dilution; Molecular Probes) was applied for 1 h at 21 °C. Cell

nuclei were contrast-stained by incubation with 1 μM TO-PRO 3-iodide solution (Molecular Probes) for 5 min prior to mounting. After washing three times with 2× PBS, the coverslips were mounted on microscope slides in AntiFade mounting solution (Molecular Probes, Inc.).

HEK293 Cell Culture and Transfections—HEK293 cells were obtained from ATCC and cultured in DMEM supplemented with 10% FBS (Omega Scientific) according to ATCC recommendations. Transfections of cDNA were performed using Lipofectamine 2000 reagent (Invitrogen). Plasmid containing the full-length mouse RyR2 coding sequence fused with the yellow fluorescent protein (YFP) coding sequence inserted after Ser-437 ($RyR2_{S437}$-YFP construct) (33, 34) was obtained from Dr. S. R. Wayne Chen (University of Calgary). Insertion of YFP after Ser-437 has little effect on the structure and function of the heterologously expressed RyR2 (33, 34). Cherry-STIM1 plasmid (35) was obtained from Dr. Richard S. Lewis (Stanford University).

Confocal Imaging—Fluorescence images of fixed or living cells were acquired using an LSM 510 laser-scanning confocal imaging system (Carl Zeiss) via a ×63/1.4 numerical aperture oil immersion objective. The excitation/emission settings were as follows: 488-nm line of excitation and 505–550-nm emission filter for Alexa Fluor 488 and $RyR2_{S437}$-YFP; 543-nm line of excitation and a 560-nm longpass emission filter for Cherry-STIM1; and 633-nm line of excitation and a 650-nm longpass emission filter for TO-PRO 3-iodide. Images of TO-PRO 3-iodide and Alexa Fluor 488 or of Cherry-STIM1 and $RyR2_{S437}$-YFP were obtained in red and green channels, respectively, by sequential scanning of the same area. In each set of experiments, optical sections were acquired using the identical image acquisition settings.

Immunofluorescence and Co-localization Analyses—Mean Alexa Fluor 488 fluorescence values were measured from confocal images recorded in green channel using ImageJ software. The background-subtracted Alexa Fluor 488 signal values were normalized to a total number of cells in each image. Object-based co-localization analyses of confocal images recorded in red and green channels were performed using the JACoP plug-in of ImageJ software as described previously (36). Briefly, the threshold was automatically adjusted by the software for each color channel. Objects with a size of ≥0.2 μm^2 and circularity ($4\pi \times$ (area/perimeter^2)) of ≥0.4 were automatically identified in each color channel by detecting the rapid intensity variations (see supplemental material). The number of individual objects and the area occupied by each object were determined by software in both color channels. A region of interest only composed of structural pixels present in both channels was created, and the correlation of fluorescence signals in both channels was explored only within this region of interest. Object-based nearest neighbor distance and centers-particles coincidence co-localization analyses were performed.

Cell Proliferation Assay—A cell division track assay was performed using the CellTrace carboxyfluorescein diacetate succinimidyl ester (CFSE) cell proliferation kit (Invitrogen) as described previously (19). Briefly, resting T cells were washed, resuspended in PBS containing 4 μM CFSE at a density of 1×10^6 cells/ml, and incubated at 37 °C for 10 min. Labeling was quenched by adding five volumes of cold RPMI 1640 culture medium containing 10% FBS (Omega Scientific). A portion of the CFSE-labeled resting T cells was washed three times with RPMI 1640 plus 10% FBS, centrifuged, fixed with 1% paraformaldehyde in PBS, and then analyzed by flow cytometry to establish the CFSE fluorescence profile of undivided cells. The remaining CFSE-labeled resting T cells were resuspended in cell culture medium at a density of 0.05×10^6 cells/ml and divided into four groups. Each group was preincubated for 30 min at 37 °C in the presence of vehicle alone (DMSO or methanol; controls), Ry (400 μM), or DS (30 μM). Cells were then activated with anti-CD3/CD28 mAb for 4 days in the continuous presence of Ry, DS, or vehicle and then harvested, washed with PBS, and fixed with 1% paraformaldehyde in PBS. Cells were analyzed using a FACScan flow cytometer and CellQuest software (BD Biosciences). CFSE was excited by 488-nm light; the emitted fluorescence was collected using a 505–550-nm bandpass filter. The data were analyzed using FlowJo software (Tree Star Inc., Ashland, OR).

$[Ca^{2+}]_i$ and Mn^{2+} Quenching Recordings—Human T cells were plated on poly-L-lysine-coated glass bottom clambers and then loaded with 1 μM Fura-2/AM and pluronic F-127 for 5 min in 2 mM Ca^{2+}-containing recording solution. After washing, cells were incubated for an additional 30 min at 37 °C in modified Tyrode's solution containing 400 μM Ry, 30 μM DS, or vehicle (methanol or DMSO). Chambers with adherent cells were mounted on the stage of a Zeiss Axiovert 200 inverted microscope (Karl Zeiss, Thornwood, NY) equipped with a SenSys CCD camera (Roper Scientific, Tucson, AZ), a 40× oil immersion Zeiss objective, and a Fura-2 filter set with a wide band emission filter (Chroma Technologies, Rockingham, VT). A Lambda DG-4 filter changer (Sutter Instruments, Novato, CA) was used for switching between 340- and 380-nm excitation wavelengths. Fura-2 fluorescence signals evoked by 340- and 380-nm excitation (F_{340} and F_{380}, respectively) were acquired every 2–8 s and every 1 s in Ca^{2+} imaging and Mn^{2+} quench experiments, respectively. Data acquisition was performed using MetaFluor version 7.0 software (Molecular Devices, Inc., Sunnyvale, CA).

In Ca^{2+} imaging experiments, the estimated $[Ca^{2+}]_i$ values were calculated from F_{340} and F_{380} values and Fura-2 calibration as described previously (19). K_d was taken as 248 nM (37). In Mn^{2+} quench experiments, levels of Ca^{2+}-independent Fura-2 fluorescence F_i were determined as $F_i = F_{340} + \alpha F_{380}$, where α is the "isocoefficient" equal to the value of the slope of the plot of F_{340} *versus* F_{380} determined experimentally, as described previously (19, 38). In each experiment, F_{340} and F_{380} fluorescence signals were acquired from 15–20 cells located in the field of view. The $[Ca^{2+}]_i$ or F_i values were calculated for each cell and then averaged for each experiment.

Recording solutions were as follows: 1) nominally Ca^{2+}-free: 130 mM NaCl, 5.6 mM KCl, 3 mM $MgCl_2$, 10 mM Na-Hepes, 10 mM D-glucose; 2) 1 mM Ca^{2+}-containing: 130 mM NaCl, 5.6 mM KCl, 1 mM $MgCl_2$, 1 mM $CaCl_2$, 10 mM Na-Hepes, 10 mM D-glucose; 3) 2 mM Ca^{2+}-containing: 130 mM NaCl, 5.6 mM KCl, 1 mM $MgCl_2$, 2 mM $CaCl_2$, 10 mM Na-Hepes, 10 mM D-glucose; 4) 10 mM Ca^{2+}-containing: 115 mM NaCl, 5.6 mM KCl, 1 mM $MgCl_2$, 10 mM $CaCl_2$, 10 mM Na-Hepes, 10 mM D-glucose; 5) 0.5

Mn^{2+} and 1 mM Ca^{2+}-containing: 130 mM NaCl, 5.6 mM KCl, 2 mM $MgCl_2$, 1 mM $CaCl_2$, 0.5 mM $MnCl_2$, 10 mM Na-Hepes, 10 mM D-glucose. The pH of all solutions was 7.3. Solution exchange was performed via a gravity-driven perfusion system that allowed for complete solution exchange in the recording chamber within 5 s. All experiments were performed at room temperature.

Sequential Store Depletion Protocol and Assessment of Store Refilling—The recording chamber with adherent cells loaded with Fura-2 was perfused for 5 min with 2 mM Ca^{2+}-containing solution and then with nominally Ca^{2+}-free bath solution for 3 min. After that, 30 μM cyclopiazonic acid (CPA) was applied in nominally Ca^{2+}-free bath solution for 10 min to deplete the store and activate store-operated plasmalemmal channels. CPA then was washed out for 10 min in nominally Ca^{2+}-free bath solution to restore sarco/endoplasmic reticulum Ca^{2+}-ATPase (SERCA) activity. Subsequently, 1, 2, or 10 mM Ca^{2+}-containing solutions were added for 1.5 min to activate SOCE. After that, nominally Ca^{2+}-free bath solution was applied to terminate SOCE, followed by application of 30 μM CPA in a Ca^{2+}-free bath solution to deplete the store after SOCE termination. Preliminary Ca^{2+} imaging experiments revealed that in control resting T cells, application of 2–10 mM Ca^{2+}-containing solution following store depletion evoked $[Ca^{2+}]_i$ transients of less than 1 μM in amplitude. In control activated T cells, application of bath solution containing ≥2 mM Ca^{2+} following store depletion evoked $[Ca^{2+}]_i$ transients of more than 1 μM in amplitude. To remain within an optimal range of Fura-2 sensitivity, in Ca^{2+} imaging experiments, we used 2–10 mM and 1 mM Ca^{2+}-containing bath solutions to induce SOCE in resting and activated T cells, respectively.

For data analysis, background-subtracted $[Ca^{2+}]_i$ transients evoked by each sequential CPA application ($[Ca^{2+}]_{i/CPA1}$, $[Ca^{2+}]_{i/CPA2}$, $[Ca^{2+}]_{i/CPA3}$, etc.) were integrated over the time in each experiment to determine the releasable store content as described previously (19, 39). Values of integrated $[Ca^{2+}]_i$ transients induced by the CPA application subsequent to the readdition of Ca^{2+}-containing bath solution were normalized to those induced by the CPA application prior to the readdition of Ca^{2+}-containing bath solution. The obtained ratio was expressed as a percentage and used as the measure of the store refilling.

$$\text{Store refilling} = \frac{\int [Ca^{2+}]_{i/CPA2}}{\int [Ca^{2+}]_{i/CPA1}} \cdot 100\% \qquad \text{(Eq. 2)}$$

Imaging of Ca^{2+} Dynamics within the ER Lumen—Jurkat YC4.2er cells stably expressing ER-targeted Ca^{2+}-sensitive yellow chameleon protein YC4.2er (40) were kindly provided by Dr. Richard S. Lewis (Stanford University). Cells were plated on a poly-L-lysine-coated glass bottom chamber mounted on a Nikon Diaphot epifluorescence microscope. Fluorescence was elicited by illumination with a 75-watt xenon lamp, and the excitation wavelength was selected at 420 ± 5 nm by a monochromator (Optoscan from Cairn Research, Faversham, UK). The fluorescence signal was collected through a ×40 objective and split by a 500-nm dichroic mirror placed at 45°. The transmitted light was passed through a 535 ± 40-nm emission filter and detected by a photomultiplier tube. The reflected fluorescence was further selected by a 480 ± 10-nm emission filter and detected by a second photomultiplier tube. Background-corrected emission fluorescence measurements acquired at 480 and 535 nm (F_{480} and F_{535}, respectively) were averaged across the 100 × 100-μm field of view to yield a raw YC4.2er chameleon protein emission ratio (F_{535}/F_{480}), which is proportional to the Ca^{2+} concentration within the ER lumen ($[Ca^{2+}]_{ER}$).

Statistical Analyses—Analyses were performed using Origin 7 software (OriginLab, Northampton, MA). All statistical data are presented as the means ± S.E., where *n* represents the number of experiments. Hypothesis testing was performed using the independent Student's *t* test.

RESULTS

RyR Expression and Function Are Up-regulated upon Primary Human T Cell Activation—To assess RyR expression and function in human T cells, we isolated resting $CD3^+$ T cells from the peripheral blood mononuclear cells of healthy volunteers. To mimic the activation of T cells that takes place during antigen presentation, we stimulated resting T cells by cross-linking CD3 and CD28 receptors with monoclonal Ab (anti-CD3/CD28 mAb), which is a commonly used approach to induce T cell activation *in vitro* (41–44). T cell activation using anti-CD3/CD28 mAb mimics the effect of APC in inducing resting T cell proliferation and cytokine production without requiring the presence of accessory cells. Resting T cells and 4–5-day activated T cells from the same donor, which were in the logarithmic phase of growth, were taken for experiments.

The abundance of *RyR1*, *RyR2*, and *RyR3* transcripts relative to a geometric average of raw C_q values of two stably expressed housekeeping genes (*B2M* and *RPL13a*) (26) were determined in resting and 5-day activated primary human T cells (Fig. 1*A*). The *RyR1*, *RyR2*, and *RyR3* transcripts were detected in all resting T cell samples. The levels of *RyR1* and *RyR2* transcripts increased by ~55- and ~12-fold, respectively, in 5-day activated T cells compared with resting T cells. The level of *RyR3* transcripts was ~100-fold lower in 5-day activated T cells than in resting T cells. Immunostaining with 34C mAb recognizing RyR1 and RyR2 produced no statistically significant signal above nonspecific background level in resting T cells (Fig. 1, *B* and *C*). In contrast, RyR1/2 immunoreactivity was present in 5-day activated T cells.

We then explored whether activation-induced up-regulation of *RyR* gene and protein expression correlates with an increase in RyR functional activity in activated T cells compared with resting cells. Intracellular Ca^{2+} imaging experiments demonstrated that application of the RyR agonist caffeine (20 mM) evoked larger amplitude $[Ca^{2+}]_i$ transients in 5-day activated T cells than in resting T cells (Fig. 1, *D* and *E*). Caffeine-induced $[Ca^{2+}]_i$ transients were inhibited by preincubating the activated T cells for 30 min with blocking concentrations of Ry (400 μM) or DS (30 μM).

One of the common ways to assess T cell activation *in vitro* is to measure T cell proliferation following T cell receptor stimulation (45). Accordingly, we investigated if RyR activity affects T cell activation using the CFSE-based proliferation assay. We found that T cell activation in the presence of Ry (400 μM) or DS

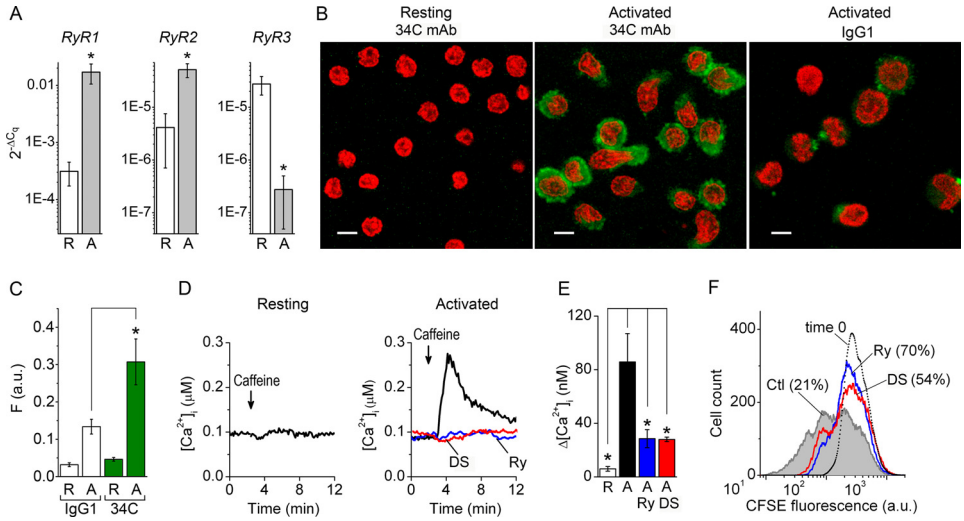

FIGURE 1. ***RyR* gene expression and function are up-regulated after T cell activation.** *A*, average normalized linearized *RyR1* (*left*), *RyR2* (*middle*), and *RyR3* (*right*) C_q values in resting T cells (*R*; $n = 9$) and 5-day activated (*A*; $n = 7$) primary human T cells. *B*, anti-RyR immunoreactivity (*green*) revealed with 34C primary mAb in resting (*left*) and 5-day activated (*middle*) T cells. *Right*, nonspecific staining of 5-day activated T cells produced by mouse IgG1 mAb (negative control). *Scale bars*, 5 μm. Optical slice depth < 4.5 μm. *C*, average levels of nonspecific background staining produced by IgG1 mAb (*open bars*) and RyR1/2 immunoreactivity detected with 34C mAb (*green bars*) in resting (*R*) and activated (*A*) T cells ($n = 8$). Before averaging, fluorescence intensities (*F*) were determined from confocal images recorded in the green channel as those shown in *B* and normalized to the number of cells in each image. *a.u.*, arbitrary units. *D*, $[Ca^{2+}]_i$ responses to caffeine (recorded from resting (*left*) and 5-day activated (*right*) T cells preincubated with vehicle (*black trace*), Ry (*blue trace*), or DS (*red trace*). Caffeine was applied as indicated. *E*, average caffeine-induced $[Ca^{2+}]_i$ transients recorded from resting T cells (*R*, *open bar*; $n = 4$), control 5-day activated T cells pretreated with vehicle alone (*Ctl*; *black bar*; $n = 7$), and activated T cells pretreated with Ry (*Ry*; *blue bar*; $n = 7$) or DS (*DS*, *red bar*; $n = 5$). Levels of $[Ca^{2+}]_i$ prior to caffeine application were subtracted before averaging. *F*, fluorescence profile of CFSE-loaded human T cells activated for 4 days in the presence of vehicle alone (*Ctl*, *gray-filled histogram*), Ry (*Ry*, *histogram outlined* by a *blue line*), or DS (*DS*, *histogram outlined* by a *red line*). The *histogram outlined* with *dots* represents the fluorescence profiles of CFSE-loaded resting T cells prior to activation (undivided cell population at time 0). The *numbers* in *parentheses* indicate a percentage of undivided cells in each group. Histogram peaks represent successive generations. Results shown are representative data from three experiments. * (in all *panels*), differences between means are significant ($p < 0.01$). *Error bars*, S.E.

(30 μM) resulted in slower expansion of activated T cells compared with control cells (Fig. 1*F*). In a control 4-day activated T cell population, 29.8 ± 6.8% ($n = 3$) of the cells were undivided. In contrast, in cell populations activated for 4 days in the presence of Ry or DS, the undivided cells accounted for 80.1 ± 10.2% ($n = 3$) and 56 ± 2.8% ($n = 3$), respectively, of total cells. Thus, all three RyR isoforms are expressed in human T cells, with RyR1 appearing to be the most abundant and most strongly up-regulated upon T cell activation. The cohort of T cell RyR receptors governs activation-induced T cell expansion.

RyR Inhibition Attenuates SOCE and Facilitates Ca^{2+} Store Refilling—Responses from Fura-2-loaded primary resting and activated T cells were evoked by a sequential store depletion protocol, which allows monitoring of the changes in $[Ca^{2+}]_i$ induced by store depletion and by SOCE in the presence of SERCA activity (Fig. 2*A*). In this protocol, 30 μM CPA, a reversible blocker of SERCA, was sequentially applied in nominally Ca^{2+}-free solution for 10 min to deplete the store and then washed out for 10 min to re-establish SERCA activity.

In resting T cells preincubated for 30 min with vehicle alone (control), Ry (400 μM), or DS (30 μM), an initial CPA application (CPA_1) evoked $[Ca^{2+}]_i$ transients due to Ca^{2+} release from the store (Fig. 2*A*). Subsequent application of 2 mM Ca^{2+}-containing bath solution evoked SOCE, which was evident from the appearance of the small amplitude $[Ca^{2+}]_i$ transients (Fig. 2, *A* and *B*). After SOCE was terminated by application of a Ca^{2+}-free bath solution, a second CPA application (CPA_2) evoked $[Ca^{2+}]_i$ transients in all groups of cells, indicating that the store was refilled during SOCE. The extent of store refilling was measured as the ratio of the integrated $[Ca^{2+}]_i$ transients evoked by CPA application after SOCE to those evoked by CPA application prior to SOCE (CPA_2/CPA_1 or CPA_3/CPA_2). In all groups of resting T cells, the store was refilled by ~50–60% of its initial releasable content during the 1.5 min of 2 mM Ca^{2+}-containing bath solution readdition (Fig. 2*D*). There were no significant differences between control cells and cells preincubated with RyR blockers in the values of store refilling following SOCE and amplitudes of $[Ca^{2+}]_i$ transients evoked by SOCE in 2 mM Ca^{2+}-containing bath solution (Fig. 2, *B* and *D*).

Application of 10 mM Ca^{2+}-containing solution following CPA wash out evoked larger amplitude $[Ca^{2+}]_i$ transients than those evoked by application of 2 mM Ca^{2+}-containing solution in control cells (Fig. 2, *A–C*). The amplitudes of the $[Ca^{2+}]_i$ transients evoked by application of 10 mM Ca^{2+}-containing solution were significantly reduced in cells preincubated with Ry or DS (Fig. 2, *A* and *C*). $[Ca^{2+}]_i$ transients evoked by CPA application following the 10 mM Ca^{2+} readdition were larger in magnitude in cells preincubated with RyR blockers than in control cells (Fig. 2*A*, *inset*). SOCE induced by the application of 10 mM Ca^{2+}-containing solution caused store refilling by less than 5% in control cells and by ~40% in cells preincubated with Ry or DS (Fig. 2*E*), indicating that enhanced SOCE evoked the Ca^{2+} release from RyR, which mitigated store refilling. Thus, functional RyR are present in resting T cells, but they are not significantly activated by SOCE alone at the physiological extracellular Ca^{2+} concentration ($[Ca^{2+}]_o$).

In activated T cells, application of 1 mM Ca^{2+}-containing solution following CPA-induced store depletion, and CPA

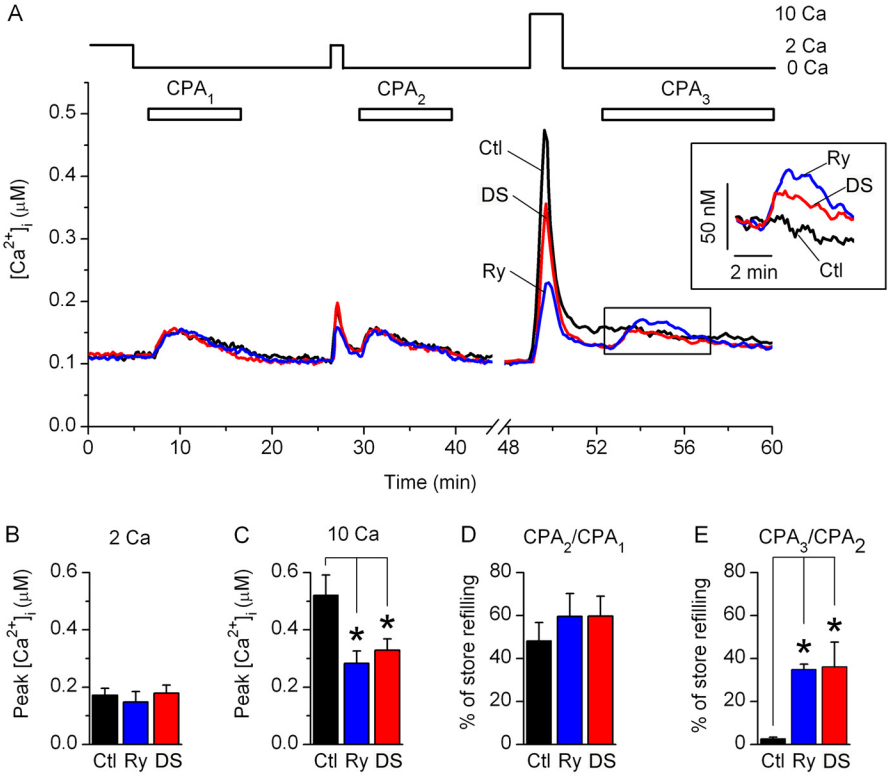

FIGURE 2. **Effects of RyR blockers on SOCE and store refilling in resting T cells.** *A*, average changes in $[Ca^{2+}]_i$ recorded from control resting T cells preincubated with vehicle alone (*Ctl*; *black trace*), Ry (*blue trace*), or DS (*red trace*). Nominally Ca^{2+}-free (0 Ca) or 2 or 10 mM Ca^{2+}-containing bath solutions (*2 Ca* and *10 Ca*, respectively) were applied as indicated. CPA was sequentially applied three times as indicated (*CPA_1*, *CPA_2*, and *CPA_3*). *Inset*, expanded *boxed area*; $[Ca^{2+}]_i$ *traces* were aligned at the time of the third CPA application. *B* and *C*, average peak values of $[Ca^{2+}]_i$ transients measured after the readdition of 2 mM (*B*) or 10 mM (*C*) Ca^{2+}-containing bath solutions in control cells (*Ctl*; *black bars*) and in cells preincubated with Ry (*blue bars*) or DS (*red bars*). Levels of $[Ca^{2+}]_i$ prior to the Ca^{2+} readdition were subtracted before averaging. *D* and *E*, average amount of store refilling following application of 2 mM (*CPA_2/CPA_1* in *D*) or 10 mM (*CPA_3/CPA_2* in *E*) Ca^{2+}-containing bath solution (expressed as a percentage). Store refilling values were determined in control cells (*Ctl*; *black bars*) and in cells preincubated with Ry (*blue bars*) or DS (*red bars*). * (in all *panels*), differences between means are significant ($p < 0.01$). Six to seven experiments were performed for each condition. *Error bars*, S.E.

wash out evoked $[Ca^{2+}]_i$ transients that were significantly larger in amplitude than those evoked by applying 2 mM Ca^{2+}-containing solution to resting T cells (Figs. 2 (*A* and *B*) and 3 (*A* and *B*); $p < 0.01$, $n_{resting} = 7$; $n_{activated} = 15$), which is consistent with the previously reported up-regulation of SOCE in activated T cells compared with resting T cells (46, 47). Amplitudes of the SOCE-induced $[Ca^{2+}]_i$ transients were significantly reduced, whereas SOCE-induced store refilling was enhanced in activated T cells preincubated with RyR blockers compared with control activated T cells (Fig. 3, *A–C*). Thus, in activated T cells, RyR activity significantly affects the magnitude of SOCE and the extent of store refilling at physiological $[Ca^{2+}]_o$.

The inverse relationships between the amplitude of SOCE-triggered $[Ca^{2+}]_i$ transients and the extent of the SOCE-induced store refilling (Figs. 2 (*A*, *C*, and *E*) and 3 (*A*, *B*, and *C*)) suggest that RyR activation facilitates SOCE by reducing store-refilling following SOCE activation. To confirm that RyR activity modulates SOCE in a store-dependent manner, we examined the effects of RyR blockers on the rates of the Mn^{2+} quench of Fura-2 fluorescence in 5-day activated human T cells. The Mn^{2+} quench approach is commonly used to assess the activity of plasmalemmal store-operated Ca^{2+} channels because these channels are permeable for both Ca^{2+} and Mn^{2+}, but Mn^{2+} is not transported out of the cytosol by the plasma membrane Ca^{2+}-ATPase or SERCA. Thus, the rate of Mn^{2+} quenching provides a more accurate measure of the functional activity of store-operated Ca^{2+} channels than the rate of changes in $[Ca^{2+}]_i$ upon SOCE activation.

Prior to applying Mn^{2+}-containing bath solution, activated T cells were preincubated in Ca^{2+}-free bath solution in the presence or absence of CPA (30 μM), Ry (400 μM), or DS (30 μM). In cells that were not exposed to CPA, slow quenching of Fura-2 fluorescence was observed after application of 0.5 mM Mn^{2+}- and 1 mM Ca^{2+}-containing solution (Fig. 3*D*), due to photobleaching and Mn^{2+} entry via non-store-operated pathways. Application of 0.5 mM Mn^{2+}- and 1 mM Ca^{2+}-containing solution to the cells preincubated with CPA alone following 10 min of CPA washout in Ca^{2+}-free solution accelerated the rate of Mn^{2+} quenching (Fig. 3, *D* and *E*) due to Mn^{2+} entry via store-operated channels. Preincubation with CPA and Ry, or CPA and DS significantly decelerated the rate of Mn^{2+} quenching in CPA-treated cells. On average, the Mn^{2+} quench rate constant τ increased from 27.8 ± 2.1 s ($n = 12$) in control cells to 61.3 ± 16.1 s ($n = 6$) and 46.2 ± 6.6 s ($n = 8$) in cells pretreated with Ry or DS, respectively (Fig. 3*E*). The RyR blockers had no statistically significant effects on the Mn^{2+} quench kinetics when SERCA was permanently inhibited by inclusion of CPA in all bath solutions (Fig. 3*F*; $n = 5$), consistent with our

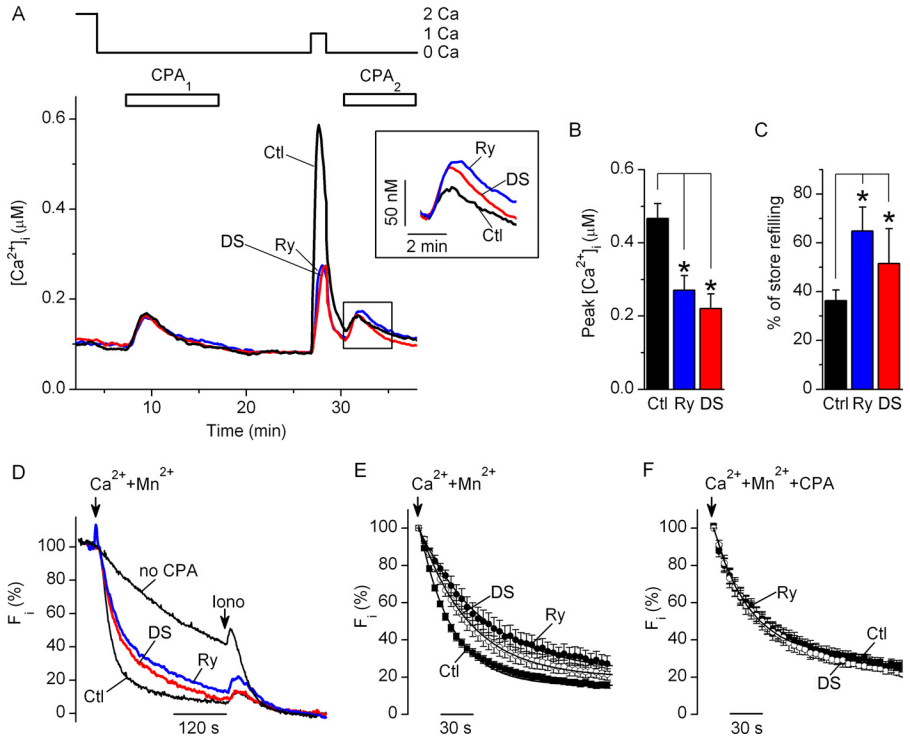

FIGURE 3. **RyR inhibition attenuates SOCE and enhances store refilling in activated T cells.** *A*, average changes in $[Ca^{2+}]_i$ recorded from the control activated T cells preincubated with vehicle alone (*Ctl*; *black trace*), Ry (*blue trace*), or DS (*red trace*). Nominally Ca^{2+}-free (0 Ca) or 1 or 2 mM Ca^{2+}-containing bath solutions (*1 Ca* and *2 Ca*, respectively) were applied as indicated. CPA was sequentially applied twice as indicated (CPA_1 and CPA_2). *Inset*, expanded *boxed area*; $[Ca^{2+}]_i$ *traces* were aligned at the time of the second CPA application. *B*, average peak values of the $[Ca^{2+}]_i$ transients after the readdition of 1 mM Ca^{2+}-containing bath solution in cells preincubated with vehicle (*Ctl*; *black bars*), Ry (*blue bars*), or DS (*red bars*). Levels of $[Ca^{2+}]_i$ prior to Ca^{2+}-containing solution readdition were subtracted before averaging. *C*, average amounts of store refilling following SOCE (expressed as a percentage) in cells preincubated with vehicle (*Ctl*; *black bars*), Ry (*blue bars*), or DS (*red bars*). *, differences between means are significant ($p < 0.05$). Thirteen to fifteen experiments were performed for each condition. *D*, representative time courses of Mn^{2+} quenching of Fura-2 fluorescence (F_i) recorded from the cells that were not treated either with CPA or RyR blockers (*no CPA*; *top black trace*) or control cells preincubated with CPA alone (*Ctl*; *bottom black trace*), CPA and Ry (*Ry*; *blue trace*), or CPA and DS (*DS*; *red trace*). All traces were recorded after 10 min of CPA washout. Ionomycin (*Iono*; 1 μM) was applied at the end of each experiment to determine the background fluorescence level. The F_i values were normalized so that the F_i values determined just before the addition of Mn^{2+} and after application of ionomycin were taken as 100 and 0%, respectively. *E* and *F*, average time courses of normalized Mn^{2+}-evoked Fura-2 quenching in cells preincubated with CPA and vehicle (*Ctl*; *filled squares*; $n = 13$ in *E*, and $n = 5$ in *F*), CPA and Ry (*Ry*; *filled circles*; $n = 6$ in *E*, and $n = 5$ in *F*), or CPA and DS (*DS*; *open circles*; $n = 8$ in *E*, and $n = 5$ in *F*). In *E*, CPA was washed out for 10 min in nominally Ca^{2+}-free bath solution before Mn^{2+} application. In *F*, CPA was continuously present in all solutions. The arrows indicate timing of application of 0.5 mM Mn^{2+}- and 2 mM Ca^{2+}-containing solution. The *solid lines* are first order exponential functions fitted to experimental data. *Error bars*, S.E.

previous results in Jurkat T cells (19). These data confirmed that in activated T cells, the RyR activity modulates SOCE via a store-dependent mechanism.

RyR Inhibition Reduces Ca^{2+} Store Leakiness and Facilitates Store Refilling—To confirm that RyR activity affects Ca^{2+} dynamics within the intracellular store during SOCE activation, we examined the changes in $[Ca^{2+}]_{ER}$ in Jurkat YC4.2er cells stably expressing ER-targeted Ca^{2+}-sensitive yellow chameleon protein YC4.2er (40). The store was depleted with 30 μM CPA, and then CPA was washed out in a nominally Ca^{2+}-free bath solution to restore SERCA activity. Activation of SOCE by the addition of 2 mM Ca^{2+}-containing bath solution caused elevation in $[Ca^{2+}]_{ER}$, which plateaued in ~1.5 min following solution exchange (Fig. 4*A*), presumably after the rates of Ca^{2+} entry into the ER and leakage from the ER are equilibrated. After removal of extracellular Ca^2, the $[Ca^{2+}]_{ER}$ declined more rapidly in control cells than in cells preincubated with Ry or DS (Fig. 4, *A* (*inset*) and *B*), indicating that the control cell ER store was leakier than that of Ry- or DS-treated cells. In addition, in control cells, the first application of Ca^{2+}-containing bath solution caused $[Ca^{2+}]_{ER}$ elevation to a lower level than the second application. In contrast, in cells preincubated with RyR blockers, the $[Ca^{2+}]_{ER}$ levels at the end of the first and second applications of Ca^{2+}-containing bath solution were comparable. These data indicate that there is ongoing store refilling in control cells with normal RyR function, but the rate of store refilling is much slower in control cells than in cells with abolished RyR activity. Thus, in Jurkat T cells, Ca^{2+} leakage from the ER store in the presence of SOCE attenuates store refilling; a large part of this leak is mediated via RyR.

RyR Co-localize with STIM1 Puncta following Store Depletion—STIM1 is an ER-resident transmembrane protein that senses changes in $[Ca^{2+}]_{ER}$ and gates CRAC channels upon change in $[Ca^{2+}]_{ER}$ (48). Store depletion triggers translocation of STIM1 proteins to the ER-plasma membrane junctional sites, where they oligomerize and form discrete puncta, which is required for CRAC channel activation (12, 35, 40, 49). We examined whether RyR co-localize with STIM1 puncta following store depletion in HEK293 cells transiently co-transfected with fluorescently tagged STIM1 (Cherry-STIM1) and RyR2 ($RyR2_{S437}$-YFP) proteins.

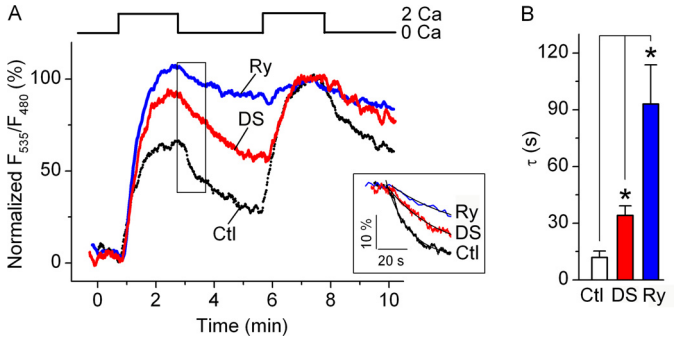

FIGURE 4. **RyR inhibition reduces Ca^{2+} leakage from the store and facilitates store refilling in Jurkat YC4.2er cells.** *A*, representative traces showing changes in $[Ca^{2+}]_{ER}$ in control cells preincubated with vehicle alone (*Ctl*; *black trace*), 400 μM Ry (*blue trace*), or 30 μM DS (*red trace*). Prior to taking measurements, the CPA was applied for 10 min and then washed out for 10 min in Ca^{2+}-free bath solution. Nominally Ca^{2+}-free (0 Ca) and 2 mM Ca^{2+}-containing (2 Ca) extracellular solutions were applied as indicated. The raw F_{535}/F_{480} values, which are proportional to $[Ca^{2+}]_{ER}$, were normalized so that F_{535}/F_{480} values determined just before the first application of 2 mM Ca^{2+}-containing solution and 1.5 min after the second application of 2 mM Ca^{2+}-containing solution were taken as 0 and 100%, respectively. *Inset*, expansion of the *boxed area*. Traces were aligned at the time of Ca^{2+}-free bath solution application. The time constant (τ) of the F_{535}/F_{480} decay was determined by fitting the initial 60-s segment of normalized F_{535}/F_{480} traces recorded following application of Ca^{2+}-free bath solution with a single exponential function (*smooth lines* in the *inset*). *B*, average values of τ obtained in control cells preincubated with vehicle alone (*Ctl*; *black bar*; $n = 9$), Ry (*blue bar*; $n = 5$), or DS (*red bar*; $n = 4$). *, differences between means are significant ($p < 0.05$). *Error bars*, S.E.

Store depletion was induced by incubating co-transfected cells for 10 min with 1 μM thapsigargin, a SERCA blocker. Confocal imaging of co-transfected cells revealed that under basal conditions, Cherry-STIM1 and $RyR2_{S437}$-YFP were localized in the tubular structures and small sized discrete puncta (Fig. 5 and supplemental material). For the purpose of quantitative analysis, we defined a punctum as an object with a size of $\geq$0.2 μm^2 and circularity of $\geq$0.4. Morphometric analysis of the puncta in images from red and green channels that record fluorescence signals from Cherry-STIM1 and $RyR2_{S437}$-YFP, respectively, revealed that the number of puncta per cell and the size of the individual punctum increased after thapsigargin-induced store depletion (Table 1 and supplemental material). To quantitatively assess the degree of Cherry-STIM1 and $RyR2_{S437}$-YFP co-localization in puncta, we performed the object-based nearest neighbor distance and centers-particles coincidence co-localization analyses (36). In nearest neighbor distance analysis, two objects from red and green channels were considered to co-localize if the distance between their geometrical centers was less than optical resolution. In centers-particles coincidence analysis, two objects from red and green channels were considered to co-localize if the geometric center of an object of the red channel fell into the area covered by an object of the green channel and *vice versa*. Both co-localization analyses revealed that the degree of Cherry-STIM1 and $RyR2_{S437}$-YFP co-localization in puncta increased significantly following

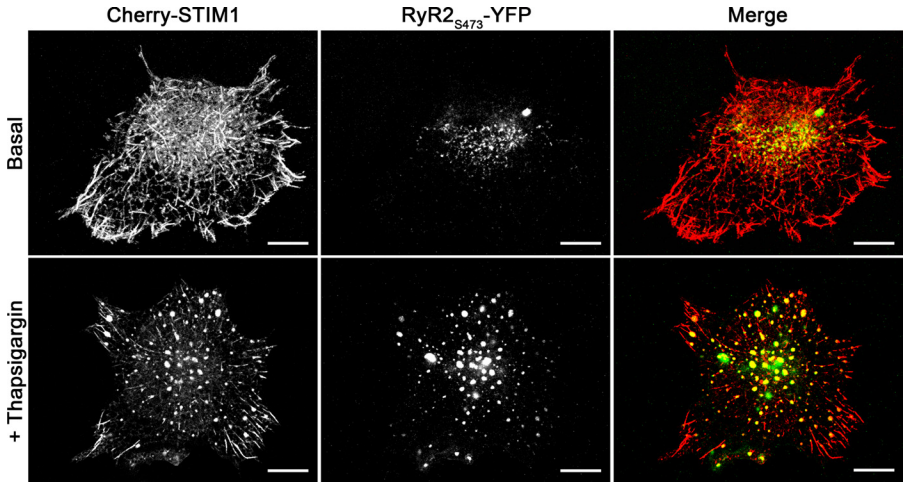

FIGURE 5. **RyR co-localize with STIM1 puncta following store depletion in HEK293 cells.** Confocal images of HEK293 cells co-overexpressing Cherry-STIM1 and $RyR2_{S437}$-YFP recorded in *red* and *green channels*, respectively, prior to store depletion (*top panels*) and 10 min following incubation in bath solution supplemented with 1 μM thapsigargin (*bottom panels*). *Right columns* show merged images of Cherry-STIM1 and $RyR2_{S437}$-YFP. Co-localization is depicted in *yellow*. *Scale bar*, 10 μm. Images were taken at the bottom of the cells; optical slice depth was <2.5 μm. Results shown are representative images from eight independent experiments.

TABLE 1
Summarized results of object-based analyses of co-localization of Cherry-STIM1 and $RyR2_{S437}$-YFP

Treatment	No. of puncta per cell[a]	Punctum area	Degree of co-localization[b]				*n*
			Geometrical centers-particles coincidence analysis		Distance between geometrical centers analysis		
			Cherry-STIM1 (red channel)	$RyR2_{S437}$-YFP (green channel)	Cherry-STIM1 (red channel)	$RyR2_{S437}$-YFP (green channel)	
		μm^2	%	%	%	%	
Vehicle	58.3 ± 16.6	0.46 ± 0.04	24.2 ± 5.2	27.7 ± 6.9	21.5 ± 3.5	27.3 ± 6.8	6
Thapsigargin	87.8 ± 34.8	1.02 ± 0.05[c]	79.7 ± 3.6[c]	79.7 ± 4.6[c]	77.8 ± 2.5[c]	68.8 ± 5.6[c]	6

[a] Total number in both red and green channels.
[b] Degree of co-localization was calculated for each channel as a percentage of puncta in the red (green) channel co-localizing with the puncta from the green (red) channel divided by the total number of all puncta from the red (green) channel.
[c] Differences between means are significant ($p < 0.001$).

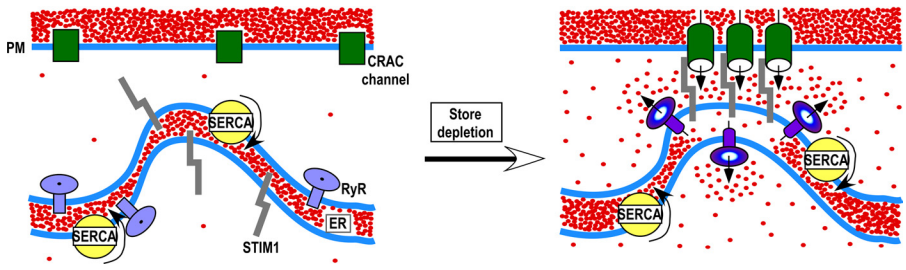

FIGURE 6. **Hypothetical scheme of RyR action in T cells.** Store depletion causes translocation of STIM1, ORAI1, and RyR to the ER-plasma membrane (*PM*) junctional sites. STIM1 interacts with ORAI1 to open CRAC channels. Ca^{2+} that entered the cell via CRAC channels activates RyR that are in close proximity to CRAC channel clusters. SERCA pumps the Ca^{2+}, which entered the cell via CRAC channels, into the ER lumen. Ca^{2+} leaks from the ER via RyR located in close proximity to STIM1. The local decline in $[Ca^{2+}]_{ER}$ in the vicinity of STIM1 Ca^{2+}-sensing domains stabilizes STIM1/ORAI1 coupling, which prevents CRAC channel inactivation in the presence of SOCE and global ER refilling.

store depletion (Table 1 and supplemental material). These data indicate that upon store depletion, both RyR and STIM1 translocate to the same ER domains and form puncta in the vicinity of the CRAC channel clusters.

DISCUSSION

The major finding of this study is that in primary human T lymphocytes, RyR control SOCE by regulating Ca^{2+} leak from the store. Because SOCE regulates a variety of Ca^{2+}-dependent T cell responses, RyR are in a position to control vital T cell functions. By extension then, RyR are potential targets for modulating immune responses in humans.

Here, we directly demonstrated that suppression of T cell RyR activity reduces the rate of SOCE in a store-dependent manner and in parallel with reducing Ca^{2+} leak from the ER. Because $[Ca^{2+}]_{ER}$ levels control CRAC channel activity such that reducing $[Ca^{2+}]_{ER}$ causes CRAC channel activation (40), whereas store refilling causes store-dependent CRAC channel inactivation (50), our data suggest that RyR activation may enhance SOCE by reducing the $[Ca^{2+}]_{ER}$ and store-dependent CRAC channel inactivation.

Co-localization of RyR and STIM1 in the puncta following store depletion provides a structural basis for the bidirectional interaction between RyR and CRAC channel machinery. It is established that translocation of STIM1 within the ER membrane to the ER-plasma membrane junctional sites, and formation of puncta following a decline in $[Ca^{2+}]_{ER}$ promotes STIM1 coupling with the CRAC channel pore-forming ORAI1 protein and CRAC channel opening (12, 48, 49, 51, 52). It was also shown that SERCA co-localize with STIM1 puncta following store depletion (53, 54). Collectively, these observations suggest that following store depletion, SOCE via CRAC channels elevates $[Ca^{2+}]_i$ at the ER-plasma membrane junctional sites, whereas SERCA absorbs Ca^{2+} that has entered the cell, resulting in an increase in $[Ca^{2+}]_{ER}$. STIM1 subsequently dissociates from the puncta, causing SOCE termination (52, 55, 56).

Co-localization of RyR with STIM1 in puncta following store depletion suggests that RyR may counterport Ca^{2+} from the junctional ER regions harboring the STIM1 Ca^{2+}-sensing domains (Fig. 6). It is possible that within the puncta, the RyR, STIM1, and CRAC channels localize in close proximity to each other but distant from SERCA. This hypothesis is supported by previous reports that RyR and SERCA may be segregated in different ER subcompartments (57, 58). Spatial co-localization of RyR, STIM1, and CRAC channels would facilitate RyR activation by SOCE via the CICR mechanism and subsequent formation of discrete microdomains of low $[Ca^{2+}]_{ER}$ ("cold spots") in the vicinity of STIM1. $[Ca^{2+}]_{ER}$ cold spots in the junctional ER compartments harboring STIM1 Ca^{2+}-sensing domains would slow down STIM1 dissociation from the puncta and CRAC channel inactivation, whereas the bulk of the ER would be refilled by SERCA. Global ER refilling may be necessary to prevent the ER stress response and for Ca^{2+} tunneling within the ER (59–61).

We have shown that transcripts of all three *RyR* family genes are expressed in primary human T cells, with *RyR1* appearing to be the most abundant. RyR1 is a predominant RyR isoform in human dendritic cells (62) and B lymphocytes (63), indicating that this isoform is preferentially expressed in primary human immune cells. Levels of *RyR1* and *RyR2* transcripts increased by 55- and 12-fold, respectively, in activated T cells compared with resting T cells. It should be noted that although T cell activation with anti-CD3/CD28 mAb is one of the commonly used methods to induce T cell activation *in vitro*, the responses obtained may be suboptimal compared with those induced with APC (44, 64). Thus, up-regulation of *RyR* gene expression upon T cell activation may be underestimated in this study. Nevertheless, it has been reported previously that a 6–10-fold increase in the expression of other genes encoding proteins involved in Ca^{2+} signaling in T cells, such as *TRPV1* (transient receptor potential vanilloid receptor 1), *TRPC3* (transient receptor potential C3-type), or *KCa3.1* (Ca^{2+}-activated K^+ channel 1.3-type), occurs under similar *in vitro* stimulation conditions (65–67). Interestingly, expression of *ORAI1* and *STIM1* genes did not change significantly (26, 65), whereas inositol 1,4,5-trisphosphate receptor (IP3R) expression was down-regulated upon T cell activation (68). Thus, RyR1 and RyR2 belong to the group of genes that are up-regulated upon T cell activation. Synergistically, up-regulated expression of the Ca^{2+} signaling proteins may account for the enhanced SOCE in activated T cells compared with resting T cells, as observed in this work and in previous studies (46, 47, 67).

Our data suggest that RyR are not functionally important in resting T cells. However, it is possible that in resting T cells, T cell receptor stimulation and production of cyclic adenosine 5′-diphosphate-ribose (20) and/or nicotinic acid adenine dinucleotide phosphate (69), the endogenous RyR agonists (70–72),

may be required to sensitize the RyR to the CICR mechanism. Furthermore, rapid CRAC channel clustering occurs at a specialized structure, called the immunological synapse, formed at the APC/T-cell interface after the T cell establishes physical contact with the APC (47, 73, 74). Upon SOCE activation, the highest level of $[Ca^{2+}]_i$ was reported to be in the vicinity of immunological synapse (47). We speculate that RyR could be recruited to the ER compartments adjacent to the immunological synapse, where they would be exposed to high $[Ca^{2+}]_i$ levels. Recruitment of RyR to the immunological synapse may facilitate RyR activation by CICR immediately after a resting T cell establishes contact with an APC.

In activated T cells, both caffeine and SOCE triggered Ca^{2+} release from the RyR in the absence of other stimuli at physiological $[Ca^{2+}]_o$, which is consistent with our previous data obtained in Jurkat T cells (19). Given that Jurkat T cells express RyR3, whereas primary human T cells predominantly express RyR1 and RyR2, we conclude that different RyR isoforms can carry out the same function in different T cell types.

We have shown previously that in Jurkat T cells, SOCE may induce CICR from both RyR and IP3R (19). CICR from IP3R potentially may account for the residual SOCE-evoked $[Ca^{2+}]_i$ transients observed in the presence of RyR inhibitors in activated T cells in this study. Because primary T cells exist in a variety of functional states characterized by the different expression levels of channels and signaling proteins, the relative contributions of RyR and IP3R in sustaining SOCE in different primary human T cell subsets would be defined by the relative expression levels of IP3R and RyR. Nevertheless, our data indicate that modulation of RyR alone significantly alters SOCE and $[Ca^{2+}]_i$ dynamics in activated T cells.

It is predictable that reduction in SOCE will attenuate activated T cell expansion. We confirmed that down-regulating SOCE by inhibiting RyR suppressed primary human T cell proliferation, consistent with previous reports (19, 20, 75). RyR have also been shown to play a role in regulating Ca^{2+} signaling and functions of human dendritic cells (62, 76, 77) and B lymphocytes (63, 78). Thus, RyR are important regulators of Ca^{2+} signaling and Ca^{2+}-dependent functions in human immune cells, which could be potentially used as a tool for modulating immune responses in humans.

Acknowledgments—We thank the staff of the University of California Davis Lucy Whittier Molecular and Diagnostic Core Facility for carrying out the RT-PCR experiments, Dr. Liudmila Zakharova for performing the proliferation assay, Dr. Sanda Despa for help with $[Ca^{2+}]_{ER}$ imaging experiments, Dr. Richard S. Lewis for providing the Jurkat YC4.2er cells and Cherry-STIM1 plasmid, Dr. S. R. Wayne Chen for providing $RyR2_{S437}$-YFP plasmid, and Dr. Jon Sack and Dr. Peter Cala for critical reading and comments on the manuscript.

REFERENCES

1. Germain, R. N. (2002) T-cell development and the CD4-CD8 lineage decision. *Nat. Rev. Immunol.* **2,** 309–322
2. Swain, S. L. (1999) Helper T cell differentiation. *Curr. Opin. Immunol.* **11,** 180–185
3. Lewis, R. S. (2001) Calcium signaling mechanisms in T lymphocytes. *Annu. Rev. Immunol.* **19,** 497–521
4. Metcalfe, J. C., Pozzan, T., Smith, G. A., and Hesketh, T. R. (1980) A calcium hypothesis for the control of cell growth. *Biochem. Soc. Symp.* **45,** 1–26
5. Crabtree, G. R. (1989) Contingent genetic regulatory events in T lymphocyte activation. *Science* **243,** 355–361
6. Crabtree, G. R., and Clipstone, N. A. (1994) Signal transmission between the plasma membrane and nucleus of T lymphocytes. *Annu. Rev. Biochem.* **63,** 1045–1083
7. Negulescu, P. A., Shastri, N., and Cahalan, M. D. (1994) Intracellular calcium dependence of gene expression in single T lymphocytes. *Proc. Natl. Acad. Sci. U.S.A.* **91,** 2873–2877
8. Negulescu, P. A., Krasieva, T. B., Khan, A., Kerschbaum, H. H., and Cahalan, M. D. (1996) Polarity of T cell shape, motility, and sensitivity to antigen. *Immunity* **4,** 421–430
9. Rao, A. (1994) NF-ATp. A transcription factor required for the coordinate induction of several cytokine genes. *Immunol. Today* **15,** 274–281
10. Datta, S., and Sarvetnick, N. (2009) Lymphocyte proliferation in immune-mediated diseases. *Trends Immunol.* **30,** 430–438
11. Karamitros, D., Kotantaki, P., Lygerou, Z., Kioussis, D., and Taraviras, S. (2011) T cell proliferation and homeostasis. An emerging role for the cell cycle inhibitor geminin. *Crit. Rev. Immunol.* **31,** 209–231
12. Hogan, P. G., Lewis, R. S., and Rao, A. (2010) Molecular basis of calcium signaling in lymphocytes. STIM and ORAI. *Annu. Rev. Immunol.* **28,** 491–533
13. Feske, S. (2011) Immunodeficiency due to defects in store-operated calcium entry. *Ann. N.Y. Acad. Sci.* **1238,** 74–90
14. Parekh, A. B. (2010) Store-operated CRAC channels. Function in health and disease. *Nat. Rev. Drug Discov.* **9,** 399–410
15. Sweeney, Z. K., Minatti, A., Button, D. C., and Patrick, S. (2009) Small-molecule inhibitors of store-operated calcium entry. *ChemMedChem* **4,** 706–718
16. Chandy, K. G., Wulff, H., Beeton, C., Pennington, M., Gutman, G. A., and Cahalan, M. D. (2004) K^+ channels as targets for specific immunomodulation. *Trends Pharmacol. Sci.* **25,** 280–289
17. Wulff, H., Beeton, C., and Chandy, K. G. (2003) Potassium channels as therapeutic targets for autoimmune disorders. *Curr. Opin. Drug Discov. Dev.* **6,** 640–647
18. Dammermann, W., Zhang, B., Nebel, M., Cordiglieri, C., Odoardi, F., Kirchberger, T., Kawakami, N., Dowden, J., Schmid, F., Dornmair, K., Hohenegger, M., Flügel, A., Guse, A. H., and Potter, B. V. (2009) NAADP-mediated Ca^{2+} signaling via type 1 ryanodine receptor in T cells revealed by a synthetic NAADP antagonist. *Proc. Natl. Acad. Sci. U.S.A.* **106,** 10678–10683
19. Dadsetan, S., Zakharova, L., Molinski, T. F., and Fomina, A. F. (2008) Store-operated Ca^{2+} influx causes Ca^{2+} release from the intracellular Ca^{2+} channels that is required for T cell activation. *J. Biol. Chem.* **283,** 12512–12519
20. Guse, A. H., da Silva, C. P., Berg, I., Skapenko, A. L., Weber, K., Heyer, P., Hohenegger, M., Ashamu, G. A., Schulze-Koops, H., Potter, B. V., and Mayr, G. W. (1999) Regulation of calcium signaling in T lymphocytes by the second messenger cyclic ADP-ribose. *Nature* **398,** 70–73
21. Schwarzmann, N., Kunerth, S., Weber, K., Mayr, G. W., and Guse, A. H. (2002) Knockdown of the type 3 ryanodine receptor impairs sustained Ca^{2+} signaling via the T cell receptor/CD3 complex. *J. Biol. Chem.* **277,** 50636–50642
22. Langhorst, M. F., Schwarzmann, N., and Guse, A. H. (2004) Ca^{2+} release via ryanodine receptors and Ca^{2+} entry. Major mechanisms in NAADP-mediated Ca^{2+} signaling in T-lymphocytes. *Cell. Signal.* **16,** 1283–1289
23. Kunerth, S., Langhorst, M. F., Schwarzmann, N., Gu, X., Huang, L., Yang, Z., Zhang, L., Mills, S. J., Zhang, L. H., Potter, B. V., and Guse, A. H. (2004) Amplification and propagation of pacemaker Ca^{2+} signals by cyclic ADP-ribose and the type 3 ryanodine receptor in T cells. *J. Cell Sci.* **117,** 2141–2149
24. Dammermann, W., and Guse, A. H. (2005) Functional ryanodine receptor expression is required for NAADP-mediated local Ca^{2+} signaling in T-lymphocytes. *J. Biol. Chem.* **280,** 21394–21399
25. Hosoi, E., Nishizaki, C., Gallagher, K. L., Wyre, H. W., Matsuo, Y., and Sei, Y. (2001) Expression of the ryanodine receptor isoforms in immune cells. *J. Immunol.* **167,** 4887–4894

26. Thakur, P., and Fomina, A. F. (2011) Density of functional Ca^{2+} release-activated Ca^{2+} (CRAC) channels declines after T-cell activation. *Channels* **5,** 510–517
27. Dolganov, G. M., Woodruff, P. G., Novikov, A. A., Zhang, Y., Ferrando, R. E., Szubin, R., and Fahy, J. V. (2001) A novel method of gene transcript profiling in airway biopsy homogenates reveals increased expression of a Na^+-K^+-Cl^- cotransporter (NKCC1) in asthmatic subjects. *Genome Res.* **11,** 1473–1483
28. Schmittgen, T. D., and Livak, K. J. (2008) Analyzing real-time PCR data by the comparative C_T method. *Nat. Protoc.* **3,** 1101–1108
29. Airey, J. A., Beck, C. F., Murakami, K., Tanksley, S. J., Deerinck, T. J., Ellisman, M. H., and Sutko, J. L. (1990) Identification and localization of two triad junctional foot protein isoforms in mature avian fast twitch skeletal muscle. *J. Biol. Chem.* **265,** 14187–14194
30. Airey, J. A., Grinsell, M. M., Jones, L. R., Sutko, J. L., and Witcher, D. (1993) Three ryanodine receptor isoforms exist in avian striated muscles. *Biochemistry* **32,** 5739–5745
31. Du, G. G., Imredy, J. P., and MacLennan, D. H. (1998) Characterization of recombinant rabbit cardiac and skeletal muscle Ca^{2+} release channels (ryanodine receptors) with a novel [^{3}H]ryanodine binding assay. *J. Biol. Chem.* **273,** 33259–33266
32. Li, P., and Chen, S. R. (2001) Molecular basis of Ca^{2+} activation of the mouse cardiac Ca^{2+} release channel (ryanodine receptor). *J. Gen. Physiol.* **118,** 33–44
33. Liu, Z., Wang, R., Tian, X., Zhong, X., Gangopadhyay, J., Cole, R., Ikemoto, N., Chen, S. R., and Wagenknecht, T. (2010) Dynamic, intersubunit interactions between the N-terminal and central mutation regions of cardiac ryanodine receptor. *J. Cell Sci.* **123,** 1775–1784
34. Wang, R., Chen, W., Cai, S., Zhang, J., Bolstad, J., Wagenknecht, T., Liu, Z., and Chen, S. R. (2007) Localization of an NH_2-terminal disease-causing mutation hot spot to the "clamp" region in the three-dimensional structure of the cardiac ryanodine receptor. *J. Biol. Chem.* **282,** 17785–17793
35. Luik, R. M., Wu, M. M., Buchanan, J., and Lewis, R. S. (2006) The elementary unit of store-operated Ca^{2+} entry. Local activation of CRAC channels by STIM1 at ER-plasma membrane junctions. *J. Cell Biol.* **174,** 815–825
36. Bolte, S., and Cordelières, F. P. (2006) A guided tour into subcellular colocalization analysis in light microscopy. *J. Microsc.* **224,** 213–232
37. Fanger, C. M., Neben, A. L., and Cahalan, M. D. (2000) Differential Ca^{2+} influx, KCa channel activity, and Ca^{2+} clearance distinguish Th1 and Th2 lymphocytes. *J. Immunol.* **164,** 1153–1160
38. Zhou, Z., and Neher, E. (1993) Mobile and immobile calcium buffers in bovine adrenal chromaffin cells. *J. Physiol.* **469,** 245–273
39. Bergling, S., Dolmetsch, R., Lewis, R. S., and Keizer, J. (1998) A fluorometric method for estimating the calcium content of internal stores. *Cell Calcium* **23,** 251–259
40. Luik, R. M., Wang, B., Prakriya, M., Wu, M. M., and Lewis, R. S. (2008) Oligomerization of STIM1 couples ER calcium depletion to CRAC channel activation. *Nature* **454,** 538–542
41. Kalamasz, D., Long, S. A., Taniguchi, R., Buckner, J. H., Berenson, R. J., and Bonyhadi, M. (2004) Optimization of human T-cell expansion *ex vivo* using magnetic beads conjugated with anti-CD3 and anti-CD28 antibodies. *J. Immunother.* **27,** 405–418
42. Levine, B. L., Bernstein, W. B., Connors, M., Craighead, N., Lindsten, T., Thompson, C. B., and June, C. H. (1997) Effects of CD28 costimulation on long-term proliferation of $CD4^+$ T cells in the absence of exogenous feeder cells. *J. Immunol.* **159,** 5921–5930
43. Sunder-Plassmann, R., Breiteneder, H., Zimmermann, K., Strunk, D., Majdic, O., Knapp, W., and Holter, W. (1996) Single human T cells stimulated in the absence of feeder cells transcribe interleukin-2 and undergo long-term clonal growth in response to defined monoclonal antibodies and cytokine stimulation. *Blood* **87,** 5179–5184
44. Geppert, T. D., and Lipsky, P. E. (1988) Activation of T lymphocytes by immobilized monoclonal antibodies to CD3. Regulatory influences of monoclonal antibodies to additional T cell surface determinants. *J. Clin. Invest.* **81,** 1497–1505
45. Kruisbeek, A. M., Shevach, E., and Thornton, A. M. (2004) Proliferative assays for T cell function. *Curr. Protoc. Immunol.*, Chapter 3, Unit 3.12
46. Fomina, A. F., Fanger, C. M., Kozak, J. A., and Cahalan, M. D. (2000) Single channel properties and regulated expression of Ca^{2+} release-activated Ca^{2+} (CRAC) channels in human T cells. *J. Cell Biol.* **150,** 1435–1444
47. Lioudyno, M. I., Kozak, J. A., Penna, A., Safrina, O., Zhang, S. L., Sen, D., Roos, J., Stauderman, K. A., and Cahalan, M. D. (2008) Orai1 and STIM1 move to the immunological synapse and are up-regulated during T cell activation. *Proc. Natl. Acad. Sci. U.S.A.* **105,** 2011–2016
48. Wu, M. M., Luik, R. M., and Lewis, R. S. (2007) Some assembly required. Constructing the elementary units of store-operated Ca^{2+} entry. *Cell Calcium* **42,** 163–172
49. Cahalan, M. D. (2009) STIMulating store-operated Ca^{2+} entry. *Nat. Cell Biol.* **11,** 669–677
50. Zweifach, A., and Lewis, R. S. (1995) Slow calcium-dependent inactivation of depletion-activated calcium current. Store-dependent and -independent mechanisms. *J. Biol. Chem.* **270,** 14445–14451
51. Liou, J., Fivaz, M., Inoue, T., and Meyer, T. (2007) Live-cell imaging reveals sequential oligomerization and local plasma membrane targeting of stromal interaction molecule 1 after Ca^{2+} store depletion. *Proc. Natl. Acad. Sci. U.S.A.* **104,** 9301–9306
52. Liou, J., Kim, M. L., Heo, W. D., Jones, J. T., Myers, J. W., Ferrell, J. E., Jr., and Meyer, T. (2005) STIM is a Ca^{2+} sensor essential for Ca^{2+} store depletion-triggered Ca^{2+} influx. *Curr. Biol.* **15,** 1235–1241
53. Alonso, M. T., Manjarrés, I. M., and García-Sancho, J. (2012) Privileged coupling between Ca^{2+} entry through plasma membrane store-operated Ca^{2+} channels and the endoplasmic reticulum Ca^{2+} pump. *Mol. Cell Endocrinol.* **353,** 37–44
54. Manjarrés, I. M., Rodríguez-García, A., Alonso, M. T., and García-Sancho, J. (2010) The sarco/endoplasmic reticulum Ca^{2+} ATPase (SERCA) is the third element in capacitative calcium entry. *Cell Calcium* **47,** 412–418
55. Smyth, J. T., Dehaven, W. I., Bird, G. S., and Putney, J. W., Jr. (2008) Ca^{2+} store-dependent and -independent reversal of Stim1 localization and function. *J. Cell Sci.* **121,** 762–772
56. Várnai, P., Tóth, B., Tóth, D. J., Hunyady, L., and Balla, T. (2007) Visualization and manipulation of plasma membrane-endoplasmic reticulum contact sites indicates the presence of additional molecular components within the STIM1-Orai1 complex. *J. Biol. Chem.* **282,** 29678–29690
57. Nori, A., Fulceri, R., Gamberucci, A., Benedetti, A., and Volpe, P. (1996) Biochemical and functional heterogeneity of rat cerebrum microsomal membranes in relation to SERCA Ca^{2+}-ATPases and Ca^{2+} release channels. *Cell Calcium* **19,** 375–381
58. Clark, J. H., Kinnear, N. P., Kalujnaia, S., Cramb, G., Fleischer, S., Jeyakumar, L. H., Wuytack, F., and Evans, A. M. (2010) Identification of functionally segregated sarcoplasmic reticulum calcium stores in pulmonary arterial smooth muscle. *J. Biol. Chem.* **285,** 13542–13549
59. Mekahli, D., Bultynck, G., Parys, J. B., De Smedt, H., and Missiaen, L. (2011) Endoplasmic-reticulum calcium depletion and disease. *Cold Spring Harb. Perspect. Biol.* **3,** a004317
60. Burdakov, D., Petersen, O. H., and Verkhratsky, A. (2005) Intraluminal calcium as a primary regulator of endoplasmic reticulum function. *Cell Calcium* **38,** 303–310
61. Petersen, O. H., and Verkhratsky, A. (2007) Endoplasmic reticulum calcium tunnels integrate signaling in polarized cells. *Cell Calcium* **42,** 373–378
62. Uemura, Y., Liu, T. Y., Narita, Y., Suzuki, M., Ohshima, S., Mizukami, S., Ichihara, Y., Kikuchi, H., and Matsushita, S. (2007) Identification of functional type 1 ryanodine receptors in human dendritic cells. *Biochem. Biophys. Res. Commun.* **362,** 510–515
63. Sei, Y., Gallagher, K. L., and Basile, A. S. (1999) Skeletal muscle type ryanodine receptor is involved in calcium signaling in human B lymphocytes. *J. Biol. Chem.* **274,** 5995–6002
64. Jenkins, M. K., Chen, C. A., Jung, G., Mueller, D. L., and Schwartz, R. H. (1990) Inhibition of antigen-specific proliferation of type 1 murine T cell clones after stimulation with immobilized anti-CD3 monoclonal antibody. *J. Immunol.* **144,** 16–22
65. Wenning, A. S., Neblung, K., Strauss, B., Wolfs, M. J., Sappok, A., Hoth, M., and Schwarz, E. C. (2011) TRP expression pattern and the functional importance of TRPC3 in primary human T-cells. *Biochim. Biophys. Acta* **1813,** 412–423
66. Ghanshani, S., Wulff, H., Miller, M. J., Rohm, H., Neben, A., Gutman,

G. A., Cahalan, M. D., and Chandy, K. G. (2000) Up-regulation of the IKCa1 potassium channel during T-cell activation. Molecular mechanism and functional consequences. *J. Biol. Chem.* **275,** 37137–37149
67. Cahalan, M. D., and Chandy, K. G. (2009) The functional network of ion channels in T lymphocytes. *Immunol. Rev.* **231,** 59–87
68. Nagaleekar, V. K., Diehl, S. A., Juncadella, I., Charland, C., Muthusamy, N., Eaton, S., Haynes, L., Garrett-Sinha, L. A., Anguita, J., and Rincón, M. (2008) IP3 receptor-mediated Ca^{2+} release in naive CD4 T cells dictates their cytokine program. *J. Immunol.* **181,** 8315–8322
69. Berg, I., Potter, B. V., Mayr, G. W., and Guse, A. H. (2000) Nicotinic acid adenine dinucleotide phosphate ($NAADP^+$) is an essential regulator of T-lymphocyte Ca^{2+} signaling. *J. Cell Biol.* **150,** 581–588
70. Zucchi, R., and Ronca-Testoni, S. (1997) The sarcoplasmic reticulum Ca^{2+} channel/ryanodine receptor. Modulation by endogenous effectors, drugs, and disease states. *Pharmacol. Rev.* **49,** 1–51
71. Fill, M., and Copello, J. A. (2002) Ryanodine receptor calcium release channels. *Physiol. Rev.* **82,** 893–922
72. Zalk, R., Lehnart, S. E., and Marks, A. R. (2007) Modulation of the ryanodine receptor and intracellular calcium. *Annu. Rev. Biochem.* **76,** 367–385
73. Dustin, M. L., Chakraborty, A. K., and Shaw, A. S. (2010) Understanding the structure and function of the immunological synapse. *Cold Spring Harb. Perspect. Biol.* **2,** a002311
74. Krummel, M. F., and Cahalan, M. D. (2010) The immunological synapse. A dynamic platform for local signaling. *J. Clin. Immunol.* **30,** 364–372
75. Gasser, A., Glassmeier, G., Fliegert, R., Langhorst, M. F., Meinke, S., Hein, D., Krüger, S., Weber, K., Heiner, I., Oppenheimer, N., Schwarz, J. R., and Guse, A. H. (2006) Activation of T cell calcium influx by the second messenger ADP-ribose. *J. Biol. Chem.* **281,** 2489–2496
76. Bracci, L., Vukcevic, M., Spagnoli, G., Ducreux, S., Zorzato, F., and Treves, S. (2007) Ca^{2+} signaling through ryanodine receptor 1 enhances maturation and activation of human dendritic cells. *J. Cell Sci.* **120,** 2232–2240
77. Vukcevic, M., Spagnoli, G. C., Iezzi, G., Zorzato, F., and Treves, S. (2008) Ryanodine receptor activation by Cav1.2 is involved in dendritic cell major histocompatibility complex class II surface expression. *J. Biol. Chem.* **283,** 34913–34922
78. Sei, Y., Gallagher, K. L., and Daly, J. W. (2001) Multiple effects of caffeine on Ca^{2+} release and influx in human B lymphocytes. *Cell Calcium* **29,** 149–160